Journal of Radiation Research, Vol. 66, No. 3, 2025, pp. 253–263
https://doi.org/10.1093/jrr/rraf021
Advance Access Publication: 30 April 2025

Investigating tumor immunogenicity as a determinant of differential abscopal effects

Yoon Seok Jeong, Kyoung Jin Lee, Yeon Ju Kim, Seung Jin Lee, Woong Sub Koom, Ik Jae Lee and Kyung Hwan Kim*

Department of Radiation Oncology, Yonsei Cancer Center, Heavy Ion Therapy Research Institute, Yonsei University College of Medicine, 50-1 Yonsei-ro, Seodaemun-gu, Seoul 03722, Republic of Korea

*Corresponding author. Department of Radiation Oncology, Yonsei Cancer Center, Heavy Ion Therapy Research Institute, Yonsei University College of Medicine, 50-1 Yonsei-ro, Seodaemun-gu, Seoul, Republic of Korea. Tel: +82-2-2228-8104; Fax: +82-2-2227-7823; Email: kyunghkim@yuhs.ac

(Received 26 December 2024; revised 18 February 2025; editorial decision 1 April 2025)

ABSTRACT

This study investigated the role of tumor immunogenicity in the ionizing radiation (IR)–induced abscopal effect. The ovalbumin-expressing B16 cell line (B16-OVA) served as a relatively immunogenic tumor model compared to the B16F10 cell line. C57BL/6 mice were implanted with B16-OVA or B16F10 in the left thigh as the primary tumor and B16F10 in the right thigh as the secondary tumor to evaluate the abscopal response. IR was applied solely to the primary tumor, followed by administration of isotype or anti-programmed cell death protein-1 (PD-1) antibodies. Tumor-infiltrating immune cells were analyzed using flow cytometry. B16-OVA tumors exhibited increased T-cell infiltration and elevated granzyme B and Ki-67 expression in $CD8^+$ T cells compared to B16F10 tumors. IR delayed secondary tumor growth in B16-OVA-irradiated mice, but not in B16F10-irradiated mice. While $CD8^+$ T-cell numbers increased in the secondary tumors of both groups, regulatory T cells significantly increased only in B16F10-irradiated mice. IR promoted differentiation from stem-like $TCF1^+TIM3^-$ to effector-like $TCF1^-TIM3^+$ $CD8^+$ T cells, with elevated granzyme B expression. Polyfunctional T cells co-expressing IFN-γ, TNF-α and IL-2 were significantly increased only in secondary tumors of B16-OVA-irradiated mice under PD-1 blockade. The abscopal effect was abolished by FTY720 treatment and $CD8^+$ T-cell depletion. In conclusion, the IR-induced abscopal effect was dependent on the immunogenicity of the irradiated tumor. The findings may have implication on enhancing abscopal effect in clinical settings.

Keywords: abscopal effect; tumor immunogenicity; ionizing radiation; immune checkpoint inhibitors; tumor-infiltrating T cells

INTRODUCTION

Ionizing radiation (IR) is known to induce immunogenic cell death, which can modulate the tumor microenvironment (TME) [1, 2]. Acting as an *in situ* vaccine, IR promotes antitumor immunity, largely driven by $CD8^+$ T cells [3, 4]. Beyond its localized effects, IR can elicit systemic immune responses, leading to the regression of distant, non-irradiated tumors, a phenomenon known as the abscopal effect [5]. Understanding the mechanisms underpinning the abscopal effect has notable clinical relevance, as it offers a foundation for developing combination therapies that integrate IR with immune checkpoint inhibitors (ICIs). Such combinations are assumed to enhance T-cell activation and counteract immune suppression, thereby amplifying antitumor responses.

In preclinical models, combining IR with ICIs has been shown to delay distant tumor growth and induce robust systemic antitumor responses [6]. However, in clinical settings, the abscopal effect remains rare, and clinical trials often fail to demonstrate substantial abscopal responses or improved outcomes despite the combined use of ICIs and IR [7]. Factors such as the sequencing of IR and ICIs and the IR dose schedule influence the abscopal effect [8, 9]. Moreover, previous studies have demonstrated that the abscopal effect depends on the immunogenicity of the irradiated tumor [10]. However, these studies often compared immunogenicity across heterogeneous cell lines with different genetic backgrounds, making it complicated to isolate the specific role of tumor immunogenicity in driving the abscopal response.

To address this limitation, we investigated the abscopal effect using the B16F10 and B16-OVA tumor models, which originate from the same parental cell line, but differ in their expression of ovalbumin (OVA), a protein that is found in egg white. OVA is a

well-characterized foreign antigen in mice that enhances T-cell-mediated immune responses and increases tumor immunogenicity, making it widely utilized in tumor models for immunological studies [11, 12]. We hypothesized that higher immunogenicity of the irradiated tumor would result in a more pronounced abscopal effect. Our results demonstrated that irradiation of the more immunogenic B16-OVA tumor induced a stronger abscopal effect on secondary B16F10 tumors compared to irradiation of B16F10 tumors. This was accompanied by increased $CD8^+$ T-cell infiltration and elevated expression of granzyme B, IFN-γ, TNF-α and IL-2 in T cells within the secondary tumors of mice with irradiated B16-OVA tumors.

MATERIALS AND METHODS

Cell lines

The B16F10 and B16-OVA cell lines, the latter expressing OVA, were used in this study. B16F10 cells were purchased from ATCC and B16-OVA cells were provided by Prof. Sang-Jun Ha (Yonsei University). B16-OVA cells were generated by transducing an OVA-expressing vector into B16F10 melanoma cells, thereby enabling stable OVA expression [11]. Both cell lines were cultured in Dulbecco's modified Eagle medium supplemented with 10% fetal bovine serum and 1% penicillin–streptomycin at 37°C in a humidified atmosphere containing 5% CO_2.

Clonogenic assay

To assess the survival fraction of B16F10 and B16-OVA cells following IR, cells were seeded in six-well plates at densities sufficient to ensure the formation of well-separated colonies and incubated overnight. Cells were then irradiated with doses of 0, 2, 4 or 6 Gy, with non-irradiated cells serving as controls. After IR, the cells were incubated for 7–14 days for colony formation, with the medium replaced every 2–3 days. Colonies were fixed using either 4% paraformaldehyde or methanol, stained with 0.5% crystal violet and air-dried. Colonies were counted and the survival fractions were calculated compared to the non-irradiated controls.

Comparison of immunogenicity of B16F10 and B16-OVA tumors

Female C57BL/6 mice (5–6 weeks old) were purchased from Orient Bio, acclimated for 1 week and maintained in accordance with institutional guidelines approved by Yonsei University's Institutional Animal Care and Use Committee (IACUC-2023-0134). For immunogenicity comparisons, mice were subcutaneously injected in the left thigh with 100 μL of Dulbecco's phosphate-buffered saline containing either 0.5×10^6 B16-OVA cells or 0.3×10^6 B16F10 cells. Mice were sacrificed once tumor sizes reached 200–300 mm^3, and tumors were harvested for flow cytometry analysis. Details on the flow cytometry analysis are provided in a separate section. In addition, an immunohistochemistry (IHC) analysis was performed to compare the density of T-cell infiltration. Tumors measuring ~200 mm^3, harvested from B16F10- or B16-OVA-implanted mice, were fixed in 4% paraformaldehyde and processed for IHC at Yonsei University. Tumor sections were deparaffinized using xylene, rehydrated in graded ethanol, washed with distilled water and subjected to antigen retrieval using Proteinase K (DAKO S3020, USA) for 10 min. Endogenous peroxidase activity was blocked with 3% hydrogen peroxide (Duksan 3059, South Korea). Primary antibodies used included anti-CD3 (SP162, Abcam, UK; 1:10) and anti-CD8α (53-6.7, eBioscience, USA; 1:100). Secondary antibodies applied were fluorescein isothiocyanate (FITC)-conjugated goat anti-rabbit IgG (ab6717, Abcam, UK; 1:200) and Alexa Fluor 594–conjugated goat anti-rat IgG (A-11007, Thermo Fisher, USA; 1:200). After thorough washing, sections were mounted using DAPI-containing medium. Imaging was performed using an Olympus BX63 microscope with CellSens Dimension software (Olympus, Japan) and a confocal microscope (LSM 700; Carl Zeiss, Germany). Filters were optimized for FITC (green) and Alexa Fluor 594 (red) to ensure specificity and minimize background noise. Quantification of $CD3^+$ and $CD8^+$ cells was carried out using ImageJ software (NIH, USA). Positive cell counts were averaged from five B16F10 tumors and four B16-OVA tumors, with three randomly selected sections analyzed per tumor to calculate the final mean.

Comparison of abscopal effects in B16F10 and B16-OVA tumors

To compare the abscopal effect induced by irradiating B16F10 or B16-OVA tumors, tumors were implanted on the bilateral thighs of female C57BL/6 mice. The tumor on the left thigh was irradiated and the tumor on the right thigh was evaluated for the abscopal effect. The B16F10 mouse model had both B16F10 tumors implanted on the bilateral thighs and the B16-OVA mouse model had the B16-OVA tumor implanted on the left side and the B16F10 tumor implanted on the opposite thigh. In detail, mice received 0.5×10^6 B16-OVA or 0.3×10^6 B16F10 cells in the left thigh. Three days later, 0.3×10^6 B16F10 cells were injected into the right thigh. IR of 10 Gy in a single fraction or sham IR was delivered to the tumor on the left thigh using the X-Rad 320 irradiator (320 kVp, 12.5 mA, 4.76 cGy/s) once the tumor size reached 200–300 mm^3. Mice were subsequently treated with 200 μg of either isotype control or anti-programmed cell death protein-1 (αPD-1) antibodies via intraperitoneal injection on the same day of IR and every alternate day for a total of three doses. Tumor sizes were monitored until either day 22 or euthanasia, which occurred when tumor volumes exceeded 2000 mm^3.

FTY720 and anti-CD8α treatment

To analyze the role of T cells in the abscopal effect observed in this study, we inhibited T-cell trafficking with FTY720 treatment. Through intraperitoneal injection, 25 μg of FTY720 (Sigma-Aldrich, USA) was administered 1 day before IR, followed by daily doses of 5 μg. Similar to the experiment performed to assess the abscopal effect, the B16F10 mouse model had both B16F10 tumors implanted on the bilateral thighs and the B16-OVA mouse model had the B16-OVA tumor implanted on the left side and the B16F10 tumor implanted on the opposite thigh. The left tumor was either sham-irradiated or received a single dose of 10 Gy. After IR, mice were treated with either isotype control or αPD-1 antibodies for a total of three doses every alternate day through intraperitoneal injection immediately after IR. Tumor size was monitored every 2–3 days.

Next, to evaluate the role of CD8 T cells on the abscopal effect, mice were treated with 200 μg of anti-CD8α antibody (Bio X Cell, USA)

1 day prior to IR and three times per week post-IR by intraperitoneal injection. The experimental design was identical to that of the FTY720 experiments. The depletion of peripheral T cells through FTY720 and depletion of $CD8^+$ T cells through anti-CD8α antibody was confirmed using flow cytometry analysis of peripheral blood.

Tumor-infiltrating T-cell analysis

To analyze tumor-infiltrating T cells, we established the same abscopal mouse model as described in the previous sections. The B16F10 mouse model had both B16F10 tumors implanted on the bilateral thighs, while the B16-OVA mouse model had B16-OVA tumors implanted on the left side and B16F10 tumors implanted on the opposite thigh. After sham irradiation or after irradiating a single dose of 10 Gy to the left thigh, a single dose of isotype control or αPD-1 antibody was administered intraperitoneally on the same day. Bilateral tumors were both harvested 3 days after and prepared for a flow cytometry analysis of the phenotype and function of tumor-infiltrating immune cells.

Flow cytometry analysis

To analyze the phenotype of tumor-infiltrating immune cells, we performed a multi-color flow cytometry analysis. Tumor tissues were dissociated into single-cell suspensions using a Gentle MACS mechanical dissociator. To block nonspecific binding, cells were incubated with TruStain FcX (BioLegend, USA). The following primary antibodies were used for staining: CD3ε (145-2C11), CD8α (53-6.7), CD19 (1D3), CD40 (3/23), CD45 (30-F11), CD24 (M1/69) and TIM-3 (RMT3-23) purchased from BD Biosciences, and CD4 (OKT4), PD-1 (29F.1A12), PD-L1 (10F.9G2), Ly6C (HK1.4), F4/80 (BM8), MHC II (M5/114.15.2), CD86 (GL-1), CD11b (M1/70), CD11c (N418) and CD103 (2E7) obtained from BioLegend. Dead cells were excluded using the LIVE/DEAD Fixable Near-IR Dead Cell Stain Kit (Invitrogen, USA). Surface staining was performed at 4°C for 20 min. For intracellular staining, the Foxp3/Transcription Factor Staining Buffer Set (eBioscience, USA) was used to stain for Ki-67 (B56), granzyme B (GzmB; GB11), Foxp3 (FJK-16s) and TCF-1/TCF7 (C63D9; Cell Signaling Technology, USA). Absolute cell counts were determined using CountBright beads (Invitrogen, USA). Flow cytometry was performed using a Lyric System (BD Biosciences, USA) and data were analyzed with FlowJo software (BD Biosciences, USA). T cells, dendritic cells (DCs) and tumor-associated macrophages (TAMs) were gated following standard protocols (Supplementary Fig. S1).

Intracellular cytokine staining

To analyze the function of tumor-infiltrating T cells, we performed intracellular cytokine staining. Single-cell suspensions obtained from tumors were treated with Cell Stimulation Cocktail (00-4970-03; Invitrogen, USA) at 37°C for 1 h and incubated with Protein Transport Inhibitor (00-4980-03; Invitrogen, USA) at 37°C for 5 h. Cells were intracellularly stained with IFN-γ (XMG1.2), TNF-α (MP6-XT22) and IL-2 (JES6-5H4) purchased from BioLegend and eBioscience.

T-Cell receptor sequencing analysis

T-Cell receptor (TCR) sequencing was conducted on abscopal model groups with B16F10 or B16-OVA tumors treated with either αPD-1 or αPD-1 + IR. DNA was extracted using the DNeasy Blood & Tissue Kit (Qiagen, Germany). Tumor samples were mixed with 200 μL of Buffer AL, incubated at 56°C for 10 min and subsequently mixed with 200 μL of ethanol. The mixture was transferred to a DNeasy Mini spin column, washed with buffers AW1 and AW2, and eluted with 200 μL of buffer AE. Sequencing of the TCRβ CDR3 regions was performed using Adaptive Immunosequencing (Adaptive Biotechnologies, USA). DNA was amplified through multiplex polymerase chain reaction and subjected to high-throughput sequencing. Unique CDR3 regions were filtered and quantified following established protocols [13–15].

Statistical analysis

Data were analyzed using GraphPad Prism 8.0 (GraphPad Software, San Diego, CA). Unpaired two-tailed *t*-tests were used for group comparisons, with statistical significance set at $P < 0.05$. Results are presented as mean ± standard deviation (SD) unless otherwise specified.

RESULTS

B16-OVA tumors exhibit characteristics of a more immunogenic tumor compared to B16F10 tumors

To assess tumor immunogenicity, we compared the tumor-infiltrating immune cells in B16F10 and B16-OVA tumors. Both tumor types exhibited similar intrinsic radiosensitivity, reflecting their shared genetic background derived from the same parental cell line (Supplementary Fig. S2). Flow cytometry analysis showed a higher frequency of T cells in B16-OVA tumors compared to that in B16F10 tumors (Fig. 1a), with a significantly increased number of $CD8^+$ T cells (Fig. 1b). Conversely, no significant differences were observed in the numbers of $CD4^+$ T cells (Fig. 1c), regulatory T cells (Tregs) or non-Tregs between the two tumor types (Fig. 1d and e). Immunofluorescence (IF) staining confirmed a significantly higher density of $CD3^+$ (Fig. 1f and g) and $CD8^+$ (Fig. 1f and h) cells in B16-OVA tumors, indicating enhanced T-cell infiltration in the B16-OVA TME. Merged images further validated the increased co-localization of $CD8^+$ T cells in B16-OVA tumors (Fig. 1f and i).

In addition to quantifying $CD8^+$ T cells, we evaluated their phenotypes. B16-OVA tumors contained a significantly higher frequency of $GzmB^+$ $CD8^+$ T cells (Fig. 1j), $Ki\text{-}67^+$ $CD8^+$ T cells (Fig. 1k) and $PD\text{-}1^+$ $CD8^+$ T cells (Fig. 1l). Although no differences were observed in the total numbers of DCs (Fig. 1m) or TAMs (Fig. 1n) between the groups, B16-OVA tumors exhibited an increased number of $CD40^+$ DCs (Fig. 1o) and $CD86^+$ DCs (Fig. 1p), as well as a reduced number of $PD\text{-}L1^+$ TAMs (Fig. 1q). Collectively, these findings indicate that B16-OVA tumors are more immunogenic than B16F10 tumors.

Differential abscopal effect based on the immunogenicity of the irradiated tumor

To evaluate the impact of tumor immunogenicity on the abscopal effect, we developed a tumor model with differing immunogenicity in the primary tumors using the relatively low-immunogenic B16F10 and the high-immunogenic B16-OVA tumors. We then compared the size of the secondary B16F10 tumor to assess differences in the abscopal effect (Fig. 2a and b). In the primary tumor, both the isotype control and αPD-1 antibody treatment groups exhibited tumor growth delay

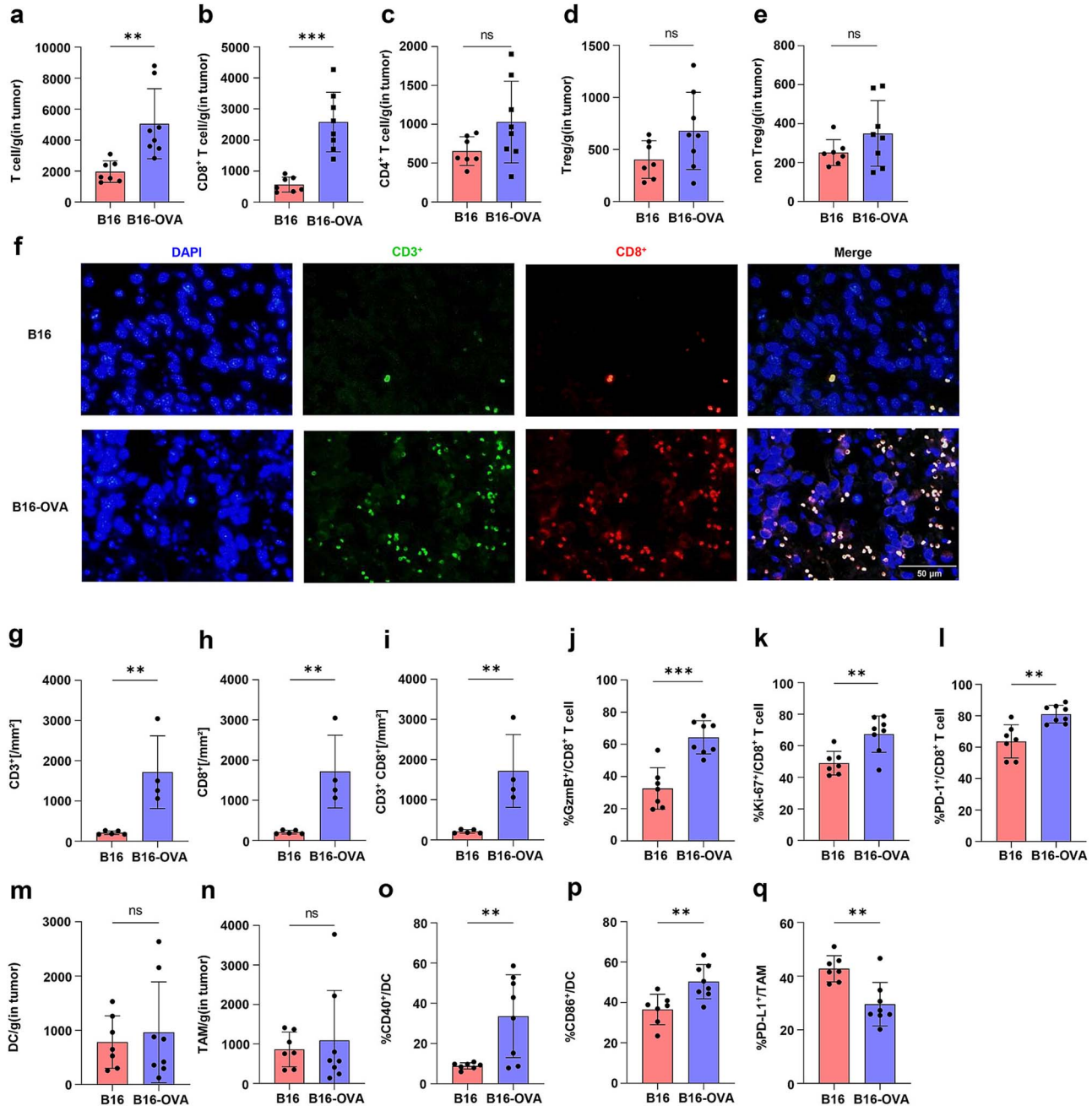

Fig. 1. Quantification and phenotypes of T-cell populations in B16F10 and B16-OVA tumors. Flow cytometry was performed on B16F10 and B16-OVA tumors of similar sizes (~200 mm³) to assess immune cell populations within the tumor microenvironment (TME). Absolute numbers per gram of tumor were determined for total T cells (a), $CD8^+$ T cells (b), $CD4^+$ T cells (c), Tregs (d) and non-Tregs (e). (f) Representative immunofluorescence (IF) staining images of $CD3^+$ and $CD8^+$ cells. Quantification of $CD3^+$ cells/mm² (g), $CD8^+$ cells/mm² (h) and merged $CD3^+CD8^+$ cells/mm² (i). Flow cytometry results showing the phenotype of $CD8^+$ T cells: proportions of $GzmB^+$ (j), Ki-67^+ (k) and PD-1^+ (l) $CD8^+$ T cells. The phenotypes of dendritic cells (DCs) (m) and tumor-associated macrophages (TAMs) (n) in both tumor types were analyzed. The proportions of DCs expressing CD40 (o) and CD86 (p) and TAMs expressing PD-L1 (q) are shown. Statistical significance is indicated (ns, not significant, $^*P < 0.05$, $^{**}P < 0.01$ and $^{***}P < 0.001$).

following IR (Fig. 2a and b, lower left panels). In secondary tumors, the abscopal effect was evaluated by comparing tumor size between IR and non-IR groups. In the B16F10 abscopal model, no significant difference was observed between the IR and non-IR groups under isotype antibody treatment (Fig. 2a, lower right panel). However, a significant difference was observed in the B16-OVA model (Fig. 2b, lower right panel). Notably, in both the B16F10 and B16-OVA abscopal models, αPD-1 antibody treatment resulted in a significant difference in secondary tumor size between IR and non-IR groups (Fig. 2a and b). The difference in secondary tumor size was 1.99-fold in the B16F10 model and 3.51-fold in the B16-OVA model. These findings indicate a more pronounced abscopal effect in the B16-OVA model.

To elucidate the mechanisms underlying the enhanced abscopal effect observed in the B16-OVA model, FTY720 was used to block T-cell egress from lymphoid organs (Fig. 3a). FTY720 was administered intraperitoneally prior to the experiment and T-cell depletion in peripheral blood was confirmed using flow cytometry (Fig. 3b). In the B16-OVA abscopal model treated with FTY720, a difference in tumor size between IR and non-IR tumors was observed in the primary tumor for both the isotype control and αPD-1 antibody–treated groups (Fig. 3a, lower left panel). However, no significant difference was observed in the secondary tumor (Fig. 3a, lower right panel).

To further investigate the role of $CD8^+$ T cells, $CD8^+$ T-cell depletion was achieved using an anti-CD8α antibody (Fig. 3c). Anti-CD8α was administered intraperitoneally before the experiment and effective depletion of $CD8^+$ T cells in peripheral blood was confirmed by flow cytometry (Fig. 3d). Similarly, in the B16-OVA abscopal model treated with anti-CD8α, a significant difference in tumor size was observed between IR and non-IR tumors in the primary tumor for both the isotype control and αPD-1 antibody-treated groups (Fig. 3c, lower left panel). However, no significant difference was observed in the secondary tumor (Fig. 3c, lower right panel). These results indicate that the abscopal effect is mediated by T cells, thus highlighting their essential role in driving this phenomenon.

Increased cytotoxic phenotype of CD8 T cells in the B16-OVA abscopal model

To assess the systemic immune response to IR, we analyzed secondary tumors. Following irradiation of the primary tumor, a significant increase in T cells (Fig. 4a) and $CD8^+$ T cells (Fig. 4b) was observed in the secondary tumor in the IR groups compared to that in the non-IR groups, except in the B16-OVA isotype group. In the B16F10 αPD-1-treated group, an increase in $CD4^+$ T cells (Fig. 4c) and Tregs (Fig. 4d) was observed in the IR group compared to that in the non-IR group, whereas non-Tregs (Fig. 4e) showed no significant change. $GzmB^+$ $CD8^+$ T cells (Fig. 4f) increased significantly in the IR group compared to that in the non-IR group in the B16-OVA αPD-1-treated group, whereas Ki-67^+ (Fig. 4g), PD-1^+ (Fig. 4h) and PD-1^+TIM-3^+ (Fig. 4i) $CD8^+$ T cells showed no significant increases. TCF-1^+TIM-3^-PD-1^+CD8^+ T cells (Fig. 4j) decreased significantly in the IR group compared to those in the non-IR group in both the B16-OVA isotype and αPD-1-treated groups. Conversely, TCF-1^-TIM-3^+PD-1^+CD8^+ T cells (Fig. 4k) increased in both groups, suggesting differentiation from stem-like T cells to terminally exhausted T cells. Notably, in the B16-OVA αPD-1-treated group, TCF-1^-TIM-3^+PD-1^+CD8^+ T cells exhibited higher GzmB expression compared to that in the TCF-1^+TIM-3^-PD-1^+CD8^+ T cells (Fig. 4l), indicating enhanced cytotoxic potential of the differentiated population. These results indicate that IR drives differentiation of TCF-1^+TIM-3^- stem-like cells into terminally differentiated cytotoxic TCF-1^-TIM-3^+ T cells. Finally, TCR sequencing of DNA from secondary tumors revealed no significant differences in Simpson clonality across treatment groups (Fig. 4m). Collectively, B16-OVA abscopal model exhibited a low Treg increase and a high expression of GzmB in $CD8^+$ T cells, indicating a more favorable antitumor response.

In the primary tumor, total T-cell counts (Fig. 5a) did not significantly differ between the IR and non-IR groups. However, in the B16F10 αPD-1 treatment group, counts of $CD8^+$ T cells (Fig. 5b), $CD4^+$ T cells (Fig. 5c), Tregs (Fig. 5d) and non-Tregs (Fig. 5e) were all significantly elevated in the IR group compared to those in the non-IR group. No significant differences were observed in the frequencies of $GzmB^+$ (Fig. 5f), Ki-67^+ (Fig. 5g), PD-1^+ (Fig. 5h) or PD-1^+TIM-3^+ (Fig. 5i) $CD8^+$ T cells between the IR and non-IR groups.

Increased T-cell functionality in B16-OVA abscopal model

Next, we evaluated T-cell functionality in the secondary tumors. The number of IFN-γ^+ $CD8^+$ T cells increased in the IR group compared to that in the non-IR group, except in the B16-OVA isotype control group (Fig. 6a and c). In the B16-OVA IR group, the number of TNF-α^+ (Fig. 6a and d) and IL-2^+ (Fig. 6a and e) $CD8^+$ T cells in the secondary tumor was significantly higher compared to that in the non-IR group. In the B16-OVA αPD-1 group, polyfunctional $CD8^+$ T cells co-expressing TNF-α^+, IL-2^+ and IFN-γ^+ were significantly increased in the IR group compared to those in the non-IR group (Fig. 6a and f). For $CD4^+$ T cells, both the B16-OVA αPD-1 and B16F10 αPD-1 groups exhibited an increase in IFN-γ^+ $CD4^+$ T cells in the IR group compared to that in the non-IR group (Fig. 6b and g). However, only the B16-OVA αPD-1 group showed a significant increase in TNF-α^+ (Fig. 6b and h) and IL-2^+ (Fig. 6b and i) $CD4^+$ T cells in the IR group compared to that in the non-IR group. Furthermore, in the secondary tumor of the B16-OVA αPD-1 group, the IR group exhibited a higher number of polyfunctional $CD4^+$ T cells compared to that in the non-IR group (Fig. 6b and j). In summary, polyfunctional $CD8^+$ and $CD4^+$ T cells were more effectively induced in the B16-OVA model.

DISCUSSION

This study demonstrated that tumor immunogenicity plays a crucial role in driving the abscopal effect. Using tumors originating from the same parental cell line but with differing immunogenicity, we showed that irradiating the relatively immunogenic B16-OVA tumor enhances the abscopal effect through increased $CD8^+$ T-cell cytotoxicity and T-cell cytokine secretion in the non-irradiated secondary tumor, compared to the less immunogenic B16F10 tumor.

Previous studies have similarly emphasized the importance of tumor immunogenicity in mediating the abscopal effect [10]. For example, Lai *et al.* compared the abscopal effect between more immunogenic MC38 and EG.7 cell lines and less immunogenic B16F10 and LLC cell lines, observing that the more immunogenic cell lines elicited a stronger abscopal response following IR. However,

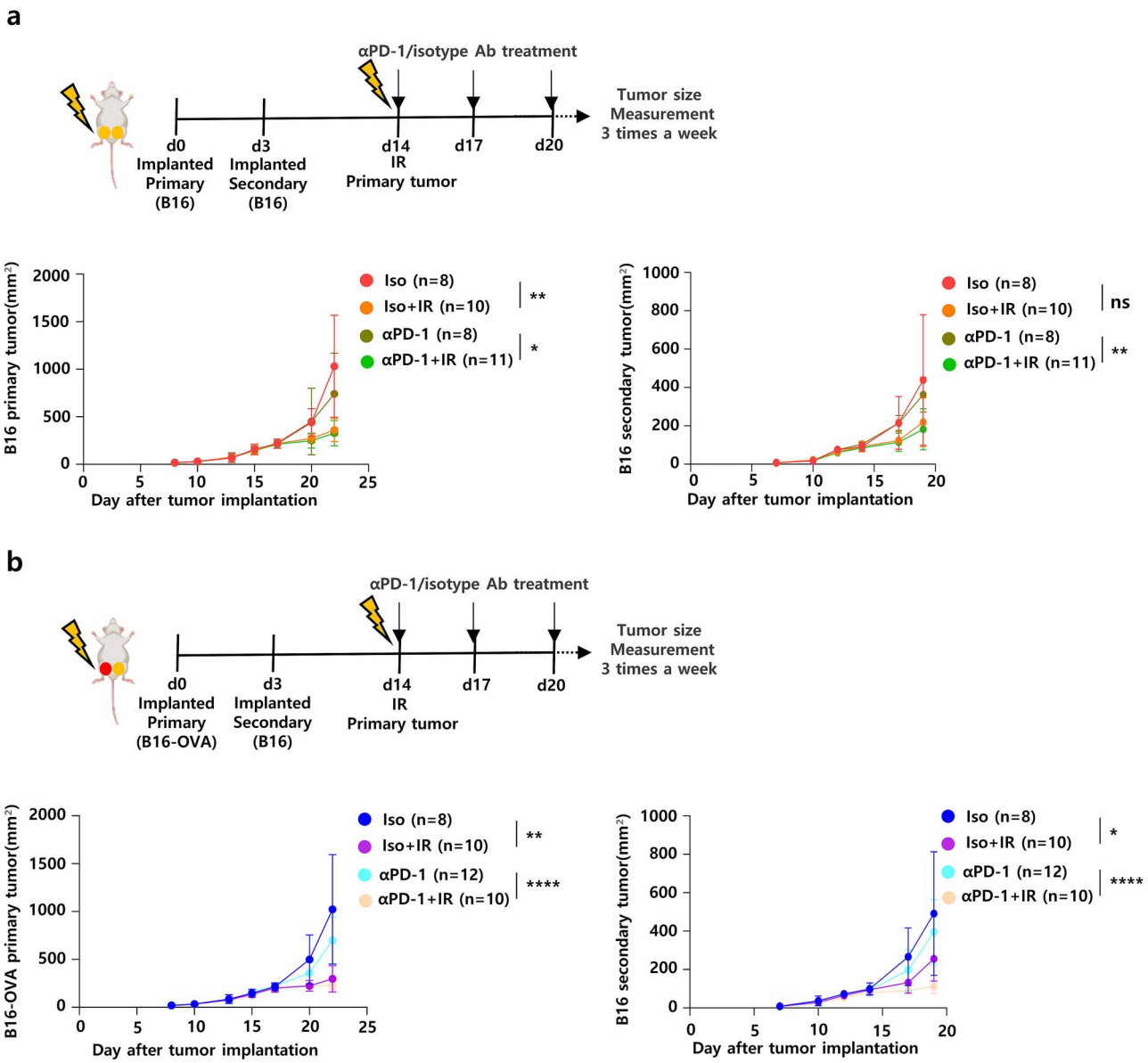

Fig. 2. Tumor growth curves of primary and secondary tumors in the abscopal model. (a) Mice were implanted with a primary B16F10 tumor in the left thigh and secondary B16F10 tumor in the right thigh 3 days later (upper panel). Tumor growth curves for the primary tumor (lower left panel) and secondary tumor (lower right panel) are shown. (b) Mice were implanted with a primary B16-OVA tumor in the left thigh and secondary B16F10 tumor in the right thigh 3 days later (upper panel). Tumor growth curves for the primary tumor (lower left panel) and secondary tumor (lower right panel) are presented. Statistical significance is indicated (ns, not significant, $^{*}P < 0.05$, $^{**}P < 0.01$ and $^{****}P < 0.0001$).

a key limitation of these studies is the potential confounding influence of other factors, such as intrinsic radiosensitivity, which can also affect the abscopal response [16]. Conversely, our study isolates the effect of tumor immunogenicity by comparing B16F10 and B16-OVA tumors, which originate from the same parental cell line and share intrinsic radiosensitivity.

After IR, we observed increased T-cell infiltration in tumors of both B16F10- and B16-OVA-irradiated mice. However, a significant increase in Tregs was observed only in the tumors of B16F10-irradiated mice, suggesting a potential suppression of $CD8^+$ and non-Treg $CD4^+$ effector T cells. Consistent with this observation, the cytokine-secreting function of $CD8^+$ and $CD4^+$ T cells was significantly enhanced only in B16-OVA-irradiated mice treated with αPD-1 therapy. Although IR induces immunogenic cell death, it can simultaneously promote immune-suppressive cell populations, such as Tregs, TAMs and myeloid-derived suppressor cells [6, 17, 18]. Our findings indicate that this immune suppression may be less pronounced when irradiating relatively immunogenic tumors.

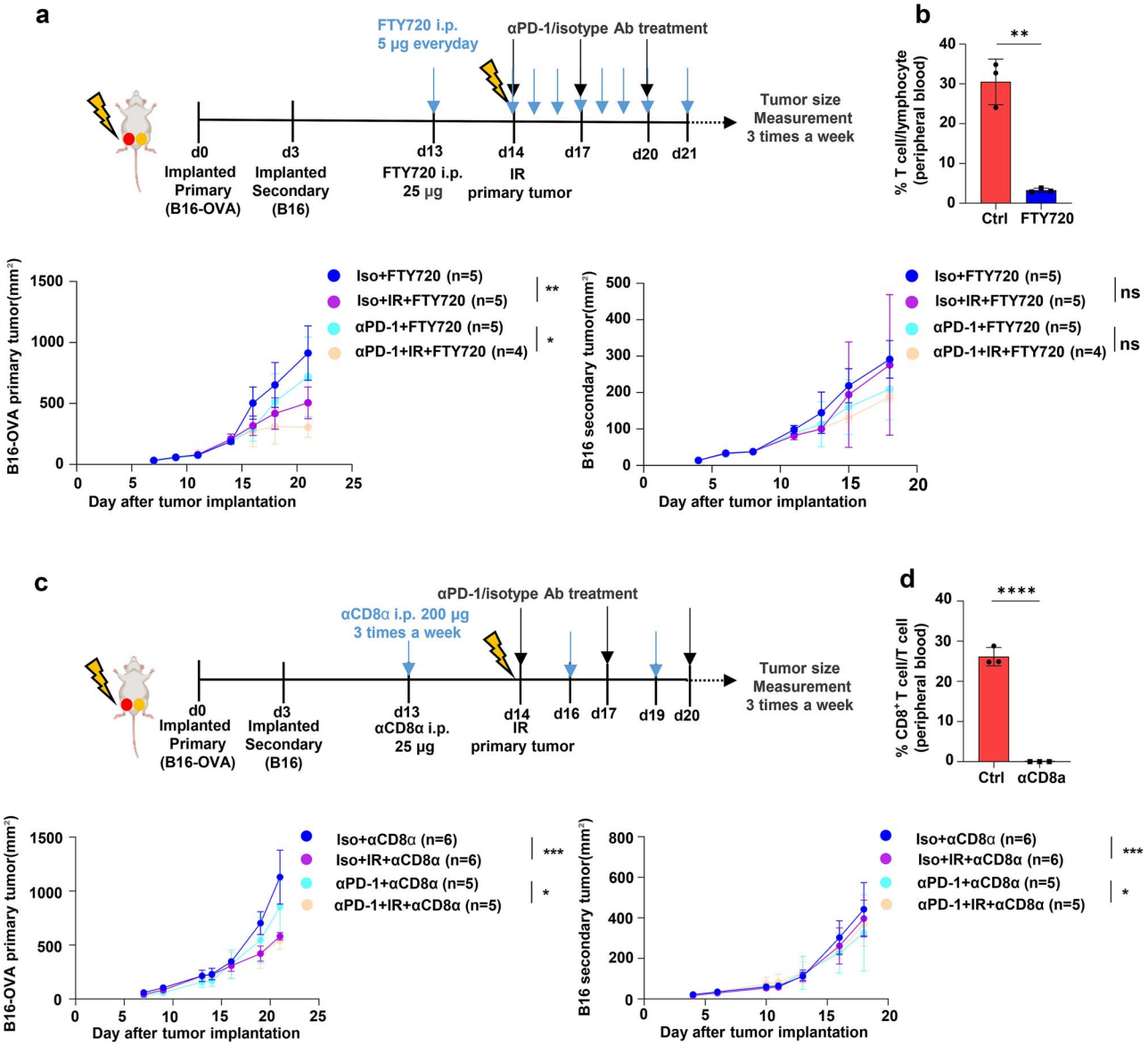

Fig. 3. FTY720 and anti-CD8α antibody treatment in the abscopal model. (a) Mice were implanted with a primary B16-OVA tumor in the left thigh and secondary B16F10 tumor in the right thigh 3 days later (upper panel). FTY720 was administered intraperitoneally daily, starting the day before IR. Peripheral T-cell counts were measured using flow cytometry (b). Tumor size comparisons for the primary tumor (lower left panel) and secondary tumor (lower right panel) are shown. (c) A similar setup was used; however, anti-CD8α was administered every 3 days, starting the day before IR (upper panel). Peripheral $CD8^+$ T-cell counts were measured by flow cytometry (d). Tumor size comparisons for the primary tumor (lower left panel) and secondary tumor (lower right panel) are presented. Statistical analysis was based on tumor size at the final measurement. Statistical significance is indicated (ns, not significant, $^*P < 0.05$, $^{**}P < 0.01$ and $^{***}P < 0.001$).

Rather than focusing solely on the quantity of T-cell infiltration, our results highlight the importance of the functional activity of tumor-infiltrating T cells in determining the abscopal response. Notably, we observed an increase in polyfunctional T cells, which secrete multiple cytokines, following the irradiation of immunogenic tumors. Additionally, granzyme B–expressing $CD8^+$ T cells were significantly increased only in the secondary tumors of B16-OVA-irradiated mice. Furthermore, we identified enhanced differentiation from stem-like $TCF1^+TIM\text{-}3^-$ to effector-like $TCF1^-TIM\text{-}3^+$ subsets among $PD\text{-}1^+CD8^+$ T cells, which exhibited higher granzyme B expression. Although $TCF1^-TIM\text{-}3^+PD\text{-}1^+CD8^+$ T cells are often considered terminally exhausted, they retain superior cytotoxic capacity to eliminate target cells [19].

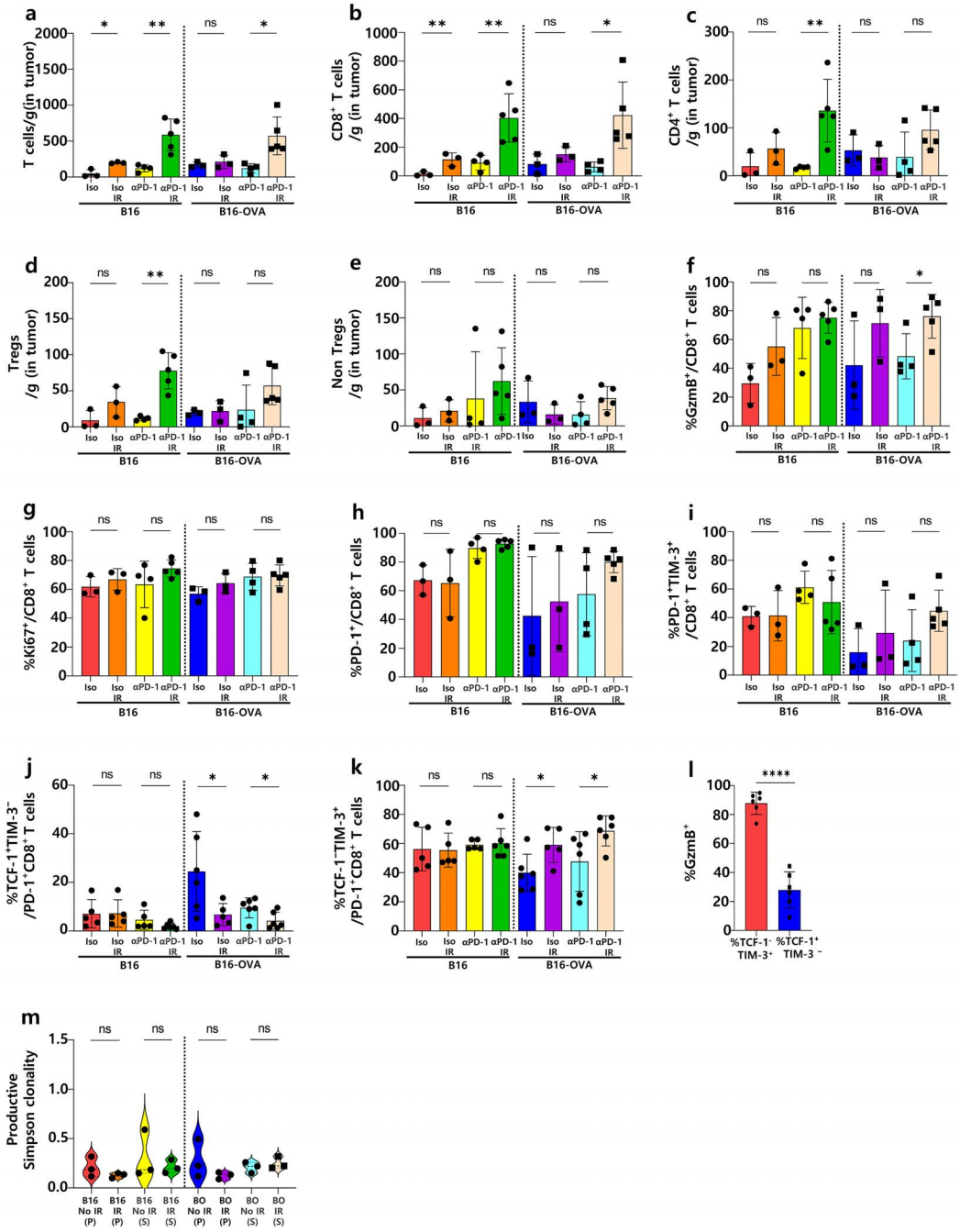

Fig. 4. Flow cytometry analysis of tumor-infiltrating T cells in secondary tumors and TCR sequencing. Mice were implanted with B16F10 or B16-OVA cells in the left thigh as the primary tumor, followed by secondary tumor implantation 3 days later. Sham irradiation or after irradiating a single dose of 10 Gy to the left thigh, a single dose of isotype control or αPD-1 antibody was administered intraperitoneally. Flow cytometry analysis was performed 3 days post-treatment. Quantification of T-cell populations in secondary B16F10 tumors: total T cells/g (a), $CD8^+$ T cells/g (b), $CD4^+$ T cells/g (c), Tregs/g (d) and non-Tregs/g (e). Phenotype analysis includes the proportions of $CD8^+$ T cells expressing $GzmB^+$ (f), $Ki\text{-}67^+$ (g), $PD\text{-}1^+$ (h) and $PD\text{-}1^+TIM\text{-}3^+$ (i). Subpopulations of $CD8^+PD\text{-}1^+$ T cells expressing $TCF\text{-}1^+TIM\text{-}3^-$ (j) or $TCF\text{-}1^-TIM\text{-}3^+$ (k) were analyzed. (l) Comparison of $GzmB^+$ expressions in $TCF\text{-}1^+TIM\text{-}3^-PD\text{-}1^+CD8^+$ and $TCF\text{-}1^-TIM\text{-}3^+PD\text{-}1^+CD8^+$ cells in secondary tumors of the B16-OVA abscopal group treated with combined anti-PD-1 and IR. (m) Productive Simpson clonality derived from TCR sequencing of B16F10 and B16-OVA tumors in the abscopal model. P refers to the primary tumor and S refers to the secondary tumor. Statistical significance is indicated (ns, not significant, $^*P < 0.05$, $^{**}P < 0.01$ and $^{****}P < 0.0001$).

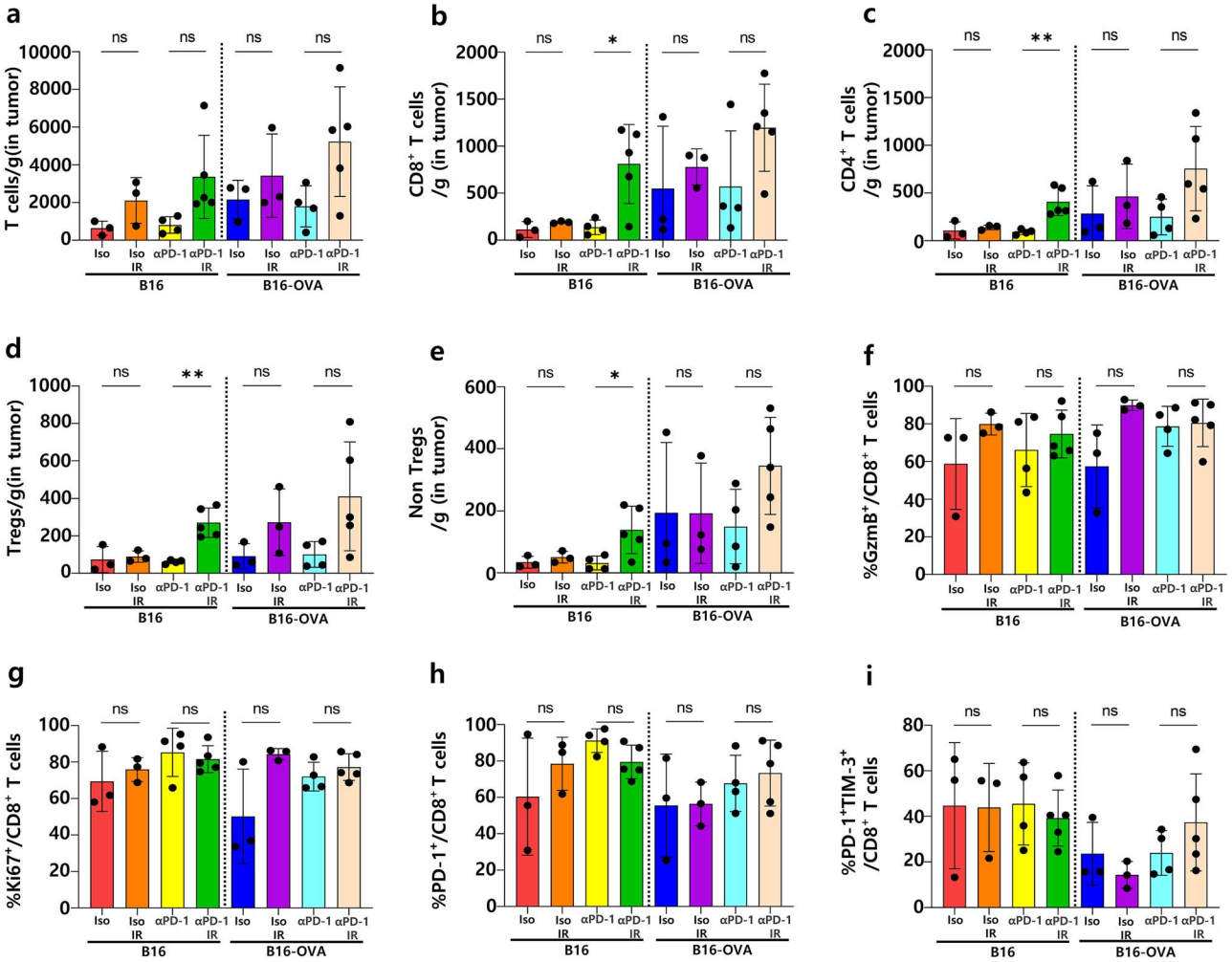

Fig. 5. Flow cytometry analysis of T-cell populations and phenotypes in primary tumors. Mice were implanted with B16F10 or B16-OVA cells in the left thigh as the primary tumor, followed by secondary tumor implantation 3 days later. Sham irradiation or after irradiating a single dose of 10 Gy to the left thigh, a single dose of isotype control or αPD-1 antibody was administered intraperitoneally. Flow cytometry analysis was performed 3 days post-treatment. Quantification of immune cells in primary B16F10 or B16-OVA tumors: total T cells/g (a), CD8$^+$ T cells/g (b), CD4$^+$ T cells/g (c), Tregs/g (d) and non-Tregs/g (e). The proportions of CD8$^+$ T cells expressing GzmB (f), Ki-67 (g) and PD-1 (h) are shown. (i) Proportion of PD-1$^+$TIM-3$^+$CD8$^+$ T cells. Statistical significance is indicated ($^*P < 0.05$, $^{**}P < 0.01$ and $^{***}P < 0.001$).

Despite the promising results seen in preclinical models, the abscopal effect remains a rare occurrence in clinical settings [7], even when ICIs are combined with IR. Optimized strategies and biomarker integration are essential to maximize the abscopal effect in clinical practice, with tumor immunogenicity emerging as a key factor. Assessing tumor immunogenicity has historically been challenging; however, recent advancements have shown that radiomic features derived from computed tomography imaging can predict CD8$^+$ T-cell infiltration [20]. These radiomic signatures have also been linked to responsiveness to ICIs [21], providing a non-invasive method to assess tumor immunogenicity and guide patient-specific strategies for inducing the abscopal effect. Such non-invasive methods when used for evaluating tumor immunogenicity may be able to prioritize a tumor among multiple tumors that should be irradiated to elicit maximal abscopal response. However, as our data have been generated from an artificial experimental system, caution is required in their interpretation and application in clinical settings.

In conclusion, this study underscores the pivotal role of tumor immunogenicity in enhancing the abscopal effect and promoting systemic antitumor responses mediated by T cells. Targeting relatively immunogenic tumors with IR may improve the likelihood of inducing abscopal effects, thus informing clinical strategies for optimizing radiotherapy in combination with ICIs. These findings emphasize the potential to enhance systemic immune activation and improve outcomes, particularly in metastatic cancer settings.

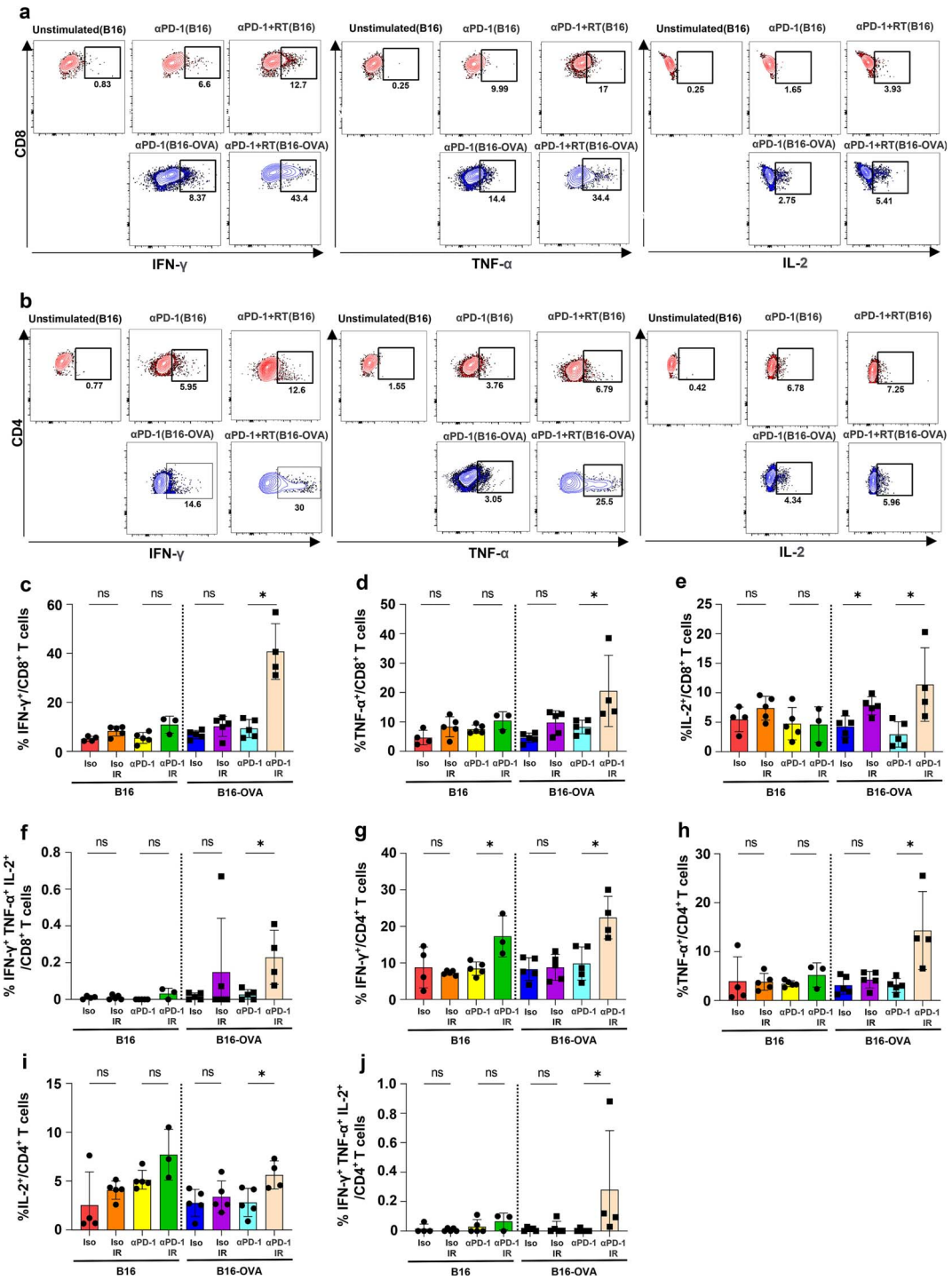

Fig. 6. Cytokine production in secondary tumors analyzed using flow cytometry. Mice were implanted with B16F10 or B16-OVA cells in the left thigh as the primary tumor, followed by secondary tumor implantation 3 days later. Sham irradiation or after irradiating a single dose of 10 Gy to the left thigh, a single dose of isotype control or αPD-1 antibody was administered intraperitoneally. Flow cytometry analysis was performed 3 days post-treatment. Representative flow cytometry plots of cytokine expression in $CD8^+$ T (a) and $CD4^+$ T (b) cells. Quantification of cytokine-producing cells: IFN-γ^+ (c), TNF-α^+ (d), IL-2^+ (e) and polyfunctional IFN-γ^+TNF-α^+IL-2^+ cells among $CD8^+$ T cells (f). Similar analysis for $CD4^+$ T cells: IFN-γ^+ (g), TNF-α^+ (h), IL-2^+ (i) and polyfunctional IFN-γ^+TNF-α^+IL-2^+ cells (j). Statistical significance is indicated (ns, not significant, $^*P < 0.05$, $^{**}P < 0.01$ and $^{***}P < 0.001$).

SUPPLEMENTARY DATA

Supplementary data is available at *Journal of Radiation Research* online.

AUTHOR CONTRIBUTIONS

Yoon Seok Jeong: formal analysis, investigation, visualization and writing—original draft. Kyoung Jin Lee: investigation, visualization and writing—review and editing. Yeon Ju Kim: investigation. Seung Jin Lee: investigation. Woong Sub Koom: resources, writing—review and editing. Ik Jae Lee: resources and writing—review and editing. Kyung Hwan Kim: conceptualization, methodology, investigation, supervision, resources, writing—review and editing, and funding acquisition.

FUNDING

This study was supported by a faculty research grant from Yonsei University College of Medicine (Grant no. 6-2021-0111) and the National Research Foundation of Korea (NRF) (Grants no. NRF-2021R1I1A1A01044024 and RS-2024-00356065).

REFERENCES

1. Sia J, Szmyd R, Hau E, Gee HE. Molecular mechanisms of radiation-induced cancer cell death: a primer. *Front Cell Dev Biol* 2020;8:41. https://doi.org/10.3389/fcell.2020.00041.
2. Galluzzi L, Vitale I, Warren S *et al.* Consensus guidelines for the definition, detection and interpretation of immunogenic cell death. *J Immunother Cancer* 2020;8:e000337. https://doi.org/10.1136/jitc-2019-000337.
3. Demaria S, Formenti SC. Role of T lymphocytes in tumor response to radiotherapy. *Front Oncol* 2012;2:95. https://doi.org/10.3389/fonc.2012.00095.
4. Lee Y, Auh SL, Wang Y *et al.* Therapeutic effects of ablative radiation on local tumor require CD8+ T cells: changing strategies for cancer treatment. *Blood* 2009;114:589–95. https://doi.org/10.1182/blood-2009-02-206870.
5. Formenti SC, Demaria S. Systemic effects of local radiotherapy. *Lancet Oncol* 2009;10:718–26. https://doi.org/10.1016/S1470-2045(09)70082-8.
6. Deng L, Liang H, Burnette B *et al.* Irradiation and anti-PD-L1 treatment synergistically promote antitumor immunity in mice. *J Clin Invest* 2014;124:687–95. https://doi.org/10.1172/JCI67313.
7. Turchan WT, Pitroda SP, Weichselbaum RR. Radiotherapy and immunotherapy combinations in the treatment of patients with metastatic disease: current status and future focus. *Clin Cancer Res* 2021;27:5188–94. https://doi.org/10.1158/1078-0432.CCR-21-0145.
8. Moore C, Hsu CC, Chen WM *et al.* Personalized ultrafractionated stereotactic adaptive radiotherapy (PULSAR) in preclinical models enhances single-agent immune checkpoint blockade. *Int J Radiat Oncol Biol Phys* 2021;110:1306–16. https://doi.org/10.1016/j.ijrobp.2021.03.047.
9. Wei J, Montalvo-Ortiz W, Yu L *et al.* Sequence of alphaPD-1 relative to local tumor irradiation determines the induction of abscopal antitumor immune responses. *Sci Immunol* 2021;6:6. https://doi.org/10.1126/sciimmunol.abg0117.
10. Lai JZ, Zhu YY, Liu Y *et al.* Abscopal effects of local radiotherapy are dependent on tumor immunogenicity. *Front Oncol* 2021;11:690188. https://doi.org/10.3389/fonc.2021.690188.
11. Lelliott EJ, Cullinane C, Martin CA *et al.* A novel immunogenic mouse model of melanoma for the preclinical assessment of combination targeted and immune-based therapy. *Sci Rep* 2019;9:1225. https://doi.org/10.1038/s41598-018-37883-y.
12. He X, Tsang TC, Luo P *et al.* Enhanced tumor immunogenicity through coupling cytokine expression with antigen presentation. *Cancer Gene Ther* 2003;10:669–77.
13. Robins HS, Campregher PV, Srivastava SK *et al.* Comprehensive assessment of T-cell receptor beta-chain diversity in alphabeta T cells. *Blood* 2009;114:4099–107. https://doi.org/10.1182/blood-2009-04-217604.
14. Carlson CS, Emerson RO, Sherwood AM *et al.* Using synthetic templates to design an unbiased multiplex PCR assay. *Nat Commun* 2013;4:2680. https://doi.org/10.1038/ncomms3680.
15. Robins H, Desmarais C, Matthis J *et al.* Ultra-sensitive detection of rare T cell clones. *J Immunol Methods* 2012;375:14–9. https://doi.org/10.1016/j.jim.2011.09.001.
16. Luke JJ, Onderdonk BE, Bhave SR *et al.* Improved survival associated with local tumor response following multisite radiotherapy and pembrolizumab: secondary analysis of a phase I trial. *Clin Cancer Res* 2020;26:6437–44. https://doi.org/10.1158/1078-0432.CCR-20-1790.
17. Sia J, Hagekyriakou J, Chindris I *et al.* Regulatory T cells shape the differential impact of radiation dose-fractionation schedules on host innate and adaptive antitumor immune defenses. *Int J Radiat Oncol Biol Phys* 2021;111:502–14. https://doi.org/10.1016/j.ijrobp.2021.05.014.
18. Reijmen E, De Mey S, De Mey W *et al.* Fractionated radiation severely reduces the number of CD8+ T cells and mature antigen presenting cells within lung tumors. *Int J Radiat Oncol Biol Phys* 2021;111:272–83. https://doi.org/10.1016/j.ijrobp.2021.04.009.
19. McLane LM, Abdel-Hakeem MS, Wherry EJ. CD8 T cell exhaustion during chronic viral infection and cancer. *Annu Rev Immunol* 2019;37:457–95. https://doi.org/10.1146/annurev-immunol-041015-055318.
20. Sun R, Limkin EJ, Vakalopoulou M *et al.* A radiomics approach to assess tumour-infiltrating CD8 cells and response to anti-PD-1 or anti-PD-L1 immunotherapy: an imaging biomarker, retrospective multicohort study. *Lancet Oncol* 2018;19:1180–91. https://doi.org/10.1016/S1470-2045(18)30413-3.
21. Sun R, Sundahl N, Hecht M *et al.* Radiomics to predict outcomes and abscopal response of patients with cancer treated with immunotherapy combined with radiotherapy using a validated signature of CD8 cells. *J Immunother Cancer* 2020;8. https://doi.org/10.1136/jitc-2020-001429.